A Method for Assimilating Lagrangian Data into a Shallow-Water-Equation Ocean Model

H. SALMAN, L. KUZNETSOV, AND C. K. R. T. JONES

Department of Mathematics, University of North Carolina at Chapel Hill, Chapel Hill, North Carolina

K. IDE

Department of Atmospheric Sciences, and Institute of Geophysics and Planetary Physics, University of California, Los Angeles, Los Angeles, California

(Manuscript received 10 January 2005, in final form 14 July 2005)

ABSTRACT

Lagrangian measurements provide a significant portion of the data collected in the ocean. Difficulties arise in their assimilation, however, since Lagrangian data are described in a moving frame of reference that does not correspond to the fixed grid locations used to forecast the prognostic flow variables. A new method is presented for assimilating Lagrangian data into models of the ocean that removes the need for any commonly used approximations. This is accomplished by augmenting the state vector of the prognostic variables with the Lagrangian drifter coordinates at assimilation. It is shown that this method is best formulated using the ensemble Kalman filter, resulting in an algorithm that is essentially transparent for assimilating Lagrangian data. The method is tested using a set of twin experiments on the shallow-water system of equations for an unsteady double-gyre flow configuration. Numerical simulations show that this method is capable of correcting the flow even if the assimilation time interval is of the order of the Lagrangian autocorrelation time scale (T_L) of the flow. These results clearly demonstrate the benefits of this method over other techniques that require assimilation times of 20%–50% of T_L, a direct consequence of the approximations introduced in assimilating their Lagrangian data. Detailed parametric studies show that this method is particularly effective if the classical ideas of localization developed for the ensemble Kalman filter are extended to the Lagrangian formulation used here. The method that has been developed, therefore, provides an approach that allows one to fully realize the potential of Lagrangian data for assimilation in more realistic ocean models.

1. Introduction

Decreasing costs in recent years has resulted in an increasing trend in the use of Lagrangian meters such as ocean drifters and floats to provide information about the ocean (Mariano et al. 2000). The realization that such meters also provide a clearer understanding of the horizontal motion of water parcels in the mesoscale range, which cannot otherwise be obtained solely from Eulerian measurements, has continued to fuel more interest in the use of such Lagrangian observations. These Lagrangian observations, for some time, were primarily used to extract statistical properties of the ocean circulation, including associated transport properties (Bauer et al. 1998; Lavender et al. 2000). This in turn has attracted ideas and techniques developed in dynamical systems theory to help quantify transport of water parcels given by the movement and interaction of coherent flow structures (Wiggins 1992; Poje and Haller 1999; Coulliette and Wiggins 2000; Kuznetsov et al. 2002). More recently, Lagrangian data have been exploited as a predictive tool rather than simply as a diagnostic tool. Carter (1989), Castellari et al. (2001), Griffa et al. (2004), Özgökmen et al. (2000, 2003), and Piterbarg (2001) carried out work along this direction in which Lagrangian data were assimilated into Lagrangian stochastic models to provide improved statistical forecasting of particle motion. Trajectories of Lagrangian tracers, however, also contain detailed quantitative information about the dynamics of the underlying flow. Noting this, several past attempts have

Corresponding author address: H. Salman, Department of Mathematics, University of North Carolina at Chapel Hill, Chapel Hill, NC 27599.
E-mail: hsalman@email.unc.edu

been conducted in order to assimilate Lagrangian data to correct the evolution of dynamical models and for estimating Eulerian velocity fields (Kamachi and O'Brien 1995; Molcard et al. 2003; Özgökmen et al. 2003). In contrast to the assimilation of Eulerian data, assimilating Lagrangian data poses several complications. The reason is that most numerical models for the ocean are solved on a fixed grid in space (Ghil and Malanotte-Rizzoli 1991), whereas the Lagrangian observations are distributed nonuniformly and do not give the data directly in terms of model variables.

Very recently, in a study conducted by Kuznetsov et al. (2003) and Ide et al. (2002), a new method was presented for assimilating Lagrangian data. The essential idea behind their approach was to augment the state space of the model by including drifter coordinates as additional variables. In so doing, an augmented error covariance matrix could be used to evolve the error correlations between the Eulerian flow variables and the Lagrangian drifter coordinates in a way that is entirely consistent with the evolution of the error correlations in Eulerian data assimilation. The resulting scheme for assimilation is in stark contrast to previous formulations to assimilate Lagrangian drifter data (see Molcard et al. 2003; Özgökmen et al. 2003). In these studies, drifters are used to derive Eulerian velocity information that was then assimilated into the Eulerian flow models. To accomplish this, they derived assimilation formulas through application of a Taylor expansion about a nondimensional time parameter that relates the observation time interval of available data to a characteristic time scale of the underlying flow. The Lagrangian assimilation schemes they adopt, therefore, introduce approximations that are above and beyond the approximations associated with Eulerian data assimilation. No such approximations are made in the approach of Kuznetsov et al. and Ide et al., thus yielding a Lagrangian data assimilation methodology in which any approximations made in assimilating Eulerian or Lagrangian data are carried out in an entirely consistent way. Furthermore, by introducing the drifters into the dynamical model and tracking them and their correlations with the flow, they were able to extract maximal information about the flow from drifter observations. An additional attractive feature of the proposed approach is the relatively straightforward implementation of the method into existing data assimilation algorithms since the augmented model approach makes the distinction between Eulerian and Lagrangian data assimilation relatively transparent. The method proposed by Kuznetsov et al. and Ide et al. was tested on point vortex systems using a Kalman filter for the assimilation step. The aim was to assimilate vortex positions that determine the state of the deterministic model flow by observing the location of Lagrangian tracers provided from another model run with stochastic forcing. Their results clearly demonstrated the success of the method in assimilating Lagrangian data. In fact, by comparing their algorithm with the aforementioned approaches, in which consecutive drifter positions are used to approximate the flow velocity, they showed that their formulation performed best for their idealized point vortex flows.

Given these recent developments, it is natural to raise the question, How well does the proposed scheme perform on flows more realistic than the point vortex systems considered by Kuznetsov et al. (2003) and Ide et al. (2002)? To address this question, we extend the formulation for the assimilation of Lagrangian data using the augmented model approach and apply it to a midlatitude ocean circulation model that comprises the classical double-gyre flow configuration (see Holland 1978). We employ a primitive equation model based on the reduced-gravity shallow-water system of equations. In a similar spirit to the work of Özgökmen et al. (2003), the reduced-gravity shallow-water system is preferred in this work over a multilayered approach for its simplicity. This avoids the need to implement specific assimilation techniques to project the surface information with fluid depth (Chin et al. 2002). However, the use of a primitive equation model is more challenging than a quasigeostrophic model as a result of the wider variability that can arise in the flow. The error correlations between each primitive variable and Lagrangian data introduce additional variability in the propagation of errors, leading to a significantly more complicated and challenging test case for assimilating Lagrangian data.

An issue that arises when employing a Kalman filter to assimilate data into a realistic model of the ocean is how to efficiently compute the evolution of the error covariance matrix. In an extended Kalman filter (EKF), which was employed by Kuznetsov et al. (2003) and Ide et al. (2002), it is common to employ the tangent linear model (TLM) to accomplish this objective. On the level of second-order statistics, it carries all the necessary information including the correlations between the errors in the flow variables and the errors in the drifter positions. We note two shortcomings of the TLM. The first is associated with the use of the TLM to evolve the error covariance matrix, which is an extremely costly computational operation. The second major shortcoming is associated with the fact that the TLM provides a linear approximation to the evolution of the covariance matrix in nonlinear systems. Therefore, for flows with significant spatial and temporal complexity arising from

the nonlinear flow model, the TLM can significantly misrepresent the evolution of the error covariance thus degrading the effectiveness of the overall algorithm. An effective alternative that overcomes these shortcomings was proposed by Evensen (1994, 2003) in the form of the ensemble Kalman filter (EnKF), which we employ in this work. Other versions of the EnKF that exist include that of Anderson (2001), Evensen and van Leeuwen (2000), and Heemink et al. (2001). The EnKF is essentially a Monte Carlo algorithm where an ensemble of model forecasts is performed from which the error covariance can be derived by construction. To obtain reasonably accurate error statistics, however, Evensen (1994) demonstrated that an ensemble of $O(100)$ members are required in typical oceanographic and meteorological applications. We can, therefore, expect our computations to involve $O(10^6)$ unknowns, which is significantly smaller than $O(10^8)$ unknowns, which would be needed to evolve only the error covariance matrix using a TLM. Another attractive feature of the EnKF is that no specific evolution operators need to be derived since we do not evolve the error covariance directly. This provides code modularity, an important feature for implementing our Lagrangian data assimilation for different models.

Our aim in this study is twofold. Our first aim is to present and test the augmented model approach for Lagrangian data assimilation in the context of an ensemble Kalman filter. Our second aim is to demonstrate the applicability of the method to assimilate Lagrangian data into flow models of the ocean. We will begin by outlining the augmented model approach for Lagrangian data assimilation, and then we will describe its formulation for an EnKF in section 2. We present our mathematical model and the flow configuration for the double gyre in section 3. Our results are presented in section 4, where the method is demonstrated within the twin-experiment framework. We also present a detailed survey regarding the dependence of the method on different assimilation parameters. We end with a summary and conclusions of the key results in section 5.

2. Ensemble Kalman filter for Lagrangian data

We begin by considering a numerical ocean model in which the state of a system is represented by the N-dimensional state vector $\mathbf{x}_F^f(t)$. The superscript f (forecast) denotes the solution given by the numerical model, and the subscript F (flow) denotes Eulerian flow variables. In general, the information contained in the state vector is dependent on the flow model and the numerical scheme used to solve the prognostic system of equations. For example, $\mathbf{x}_F^f(t)$ could contain information about the velocity field, height, salinity, etc., for each point of the grid used to discretize the flow domain. Alternatively, it can contain information about the Fourier mode coefficients for each flow variable if a spectral scheme is used. Regardless of the numerical method that is used, the size, N, of the state vector will in general correspond to the product of the number of variables and the number of discretization elements and is typically large. To represent the evolution of the flow state vector, we write

$$\frac{d\mathbf{x}_F^f}{dt} = \mathbf{m}_F(\mathbf{x}_F^f, t), \tag{1}$$

where $\mathbf{m}_F$ is the corresponding dynamics operator and is problem dependent. We will denote the corresponding state vector for the "true system" that can depend on unresolved subgrid-scale processes and other physical phenomena not represented by the dynamics operator $\mathbf{m}_F$ by $\mathbf{x}_F^t$ (Ide et al. 1997).

While precise information regarding the dynamical model may not be possible to model directly, it is possible that some statistical information regarding their properties is available. Should this be the case, then we could model $\mathbf{x}_F^t$ by a stochastic differential equation where the effect of the unmodeled processes is represented by some stochastic noise. This method in which the true system is modeled as a stochastic differential equation was employed by Kuznetsov et al. (2003). In this study, however, we will assume the true state to be governed by a deterministic equation identical to Eq. (1). The difference between the forecast and true state equations can then be obtained by simulating the same flow but with different initial conditions or model parameters. This approach is commonly referred to as the twin-experiment setup and is one that we will employ in this work. Details of how we set up our twin experiments are described in section 3.

Having defined the forecast and true models, we can now consider a set of observations $\mathbf{y}^o(t_k)$ taken at discrete time intervals t_k from the true system. We note that, in general, the dimension $\mathbf{y}^o(t_k)$ is equal to the number of observations L_k available at time t_k. For the objectives set out in this work, we will assume L_k to be constant and equal to L. In this study, we will consider the case when the observations are provided by the positions of Lagrangian drifters or floats. Therefore, at some time t_k, the horizontal positions $\mathbf{x}_D(t_k)$ of N_D drifters are observed so that we have $L = 2N_D$ observations. While the positions at a specific instant in time provide us with no information about the particular underlying flow, subsequent observations provide some information about the velocity field associated with the advec-

tion of the drifters to their new position over some time interval $[t_l, t_k]$ for $k > l$. The specific form of the equation governing the motion of a drifter will depend on the physical assumptions we employ. For now, we can express our equation as

$$\frac{d\mathbf{x}_D^f}{dt} = \mathbf{m}_D(\mathbf{x}_D^f, \mathbf{x}_F^f, t), \tag{2}$$

where $\mathbf{x}_F^f$ is given by the solution of Eq. (1). We have, therefore, assumed a one-way coupled system of equations between the flow model and the Lagrangian drifters [no dependence on $\mathbf{x}_D^f$ appears in Eq. (1)]. As before, we assume the true drifter positions to be described by an analogous evolution equation to that used for the forecast model.

Taking Eq. (1) together with Eq. (2) to describe the complete system consisting of the dynamic flow variables and the Lagrangian drifter coordinates, we can represent the state space of our model using an augmented state vector,

$$\mathbf{x} = \begin{pmatrix} \mathbf{x}_F \\ \mathbf{x}_D \end{pmatrix}. \tag{3}$$

With $\mathbf{x}_D$ now representing a subset of the state space, we can proceed to formulate a data assimilation algorithm that is transparent to the Lagrangian nature of the data we seek to assimilate into our dynamic model. Building on the recent work of Kuznetsov et al. (2003) and Ide et al. (2002), where an EKF was used to determine the analyzed state by combining observations with model predictions, we will present the augmented model approach for assimilating Lagrangian data in the context of an EnKF. To compute $\mathbf{P}^f$ using the EnKF, an ensemble of model forecasts is made from which the error covariance can be constructed. The construction of $\mathbf{P}^f$ from an ensemble prediction raises an additional difficulty, however, since we generally have no knowledge of the true state that is needed to compute the covariance. Burgers et al. (1998) noted that it is more convenient to define an ensemble covariance matrix constructed around the ensemble mean,

$$\mathbf{P}^f \approx \mathbf{P}_e^f = E[(\mathbf{x}^f - \overline{\mathbf{x}^f})(\mathbf{x}^f - \overline{\mathbf{x}^f})^{\mathrm{T}}], \tag{4}$$

where the overbar denotes an average over the ensemble,

$$\overline{\mathbf{x}^f} = \frac{1}{N_E}\sum_{j=1}^{N_E} \mathbf{x}_j^f. \tag{5}$$

The ensemble covariance can then be defined as in Burgers et al.:

$$\mathbf{P}_e^f = \frac{1}{N_E - 1}\sum_{j=1}^{N_E} (\mathbf{x}_j^f - \overline{\mathbf{x}^f})(\mathbf{x}_j^f - \overline{\mathbf{x}^f})^{\mathrm{T}}. \tag{6}$$

The key point to note is that since each ensemble member is evolved using the fully nonlinear system of equations given by Eqs. (1) and (2), nonlinear effects for the evolution of the covariance matrix are included in the EnKF. This property makes the EnKF more appropriate for use in highly nonlinear systems, such as the shallow-water equations we investigate in this study, than the EKF. The main source of error in the EnKF, however, arises from the use of a finite number of ensembles to represent the error statistics and the mean of the forecast. The errors associated with this truncation will generally decrease as the ensemble size increases. However, to apply the EnKF in model predictions of the ocean, it is unrealistic to use a very large ensemble size due to the computational costs involved. We will, therefore, test the scheme using an ensemble size of $O(80)$ members or less to assess the feasibility of our Lagrangian data assimilation algorithm with the EnKF.

Having defined the error covariance matrix with Eqs. (5)–(6), we can now construct a first-order approximation to an optimum analysis state through

$$\mathbf{x}_j^a(t_k) = \mathbf{x}_j^f(t_k) + \mathbf{K}(t_k)\mathbf{d}_j(t_k), \tag{7}$$

where the superscript a refers to the assimilated state and the subscript j denotes an individual member from our ensemble forecast. The update for each ensemble member can therefore be interpreted as a linear combination of the model forecast, $\mathbf{x}_j^f$, and the product of the innovation vector (the L dimensional vector of differences between the observations and the prediction of observed quantities by the model)

$$\mathbf{d}_j(t_k) = \mathbf{y}^o(t_k) - \mathbf{H}\mathbf{x}_j^f(t_k) + \widetilde{\boldsymbol{\epsilon}_j^f}(t_k), \tag{8}$$

and the Kalman gain matrix defined as

$$\mathbf{K} = \mathbf{P}_e^f\mathbf{H}^{\mathrm{T}}(\mathbf{H}\mathbf{P}_e^f\mathbf{H}^{\mathrm{T}} + \mathbf{R}_e)^{-1}. \tag{9}$$

In Eq. (9), the arguments have been dropped for brevity. A particularly important feature to note from our formulation is that the augmented model results in an extremely simple form for the forward observation operator, which in block form is

$$\mathbf{H} = (\mathbf{0} \quad \mathbf{I}). \tag{10}$$

Here $\mathbf{0}$ is an $L \times N$ matrix of zeros and $\mathbf{I}$ is an $L \times L$ unit matrix. Therefore, assimilating Lagrangian data by means of an augmented model eliminates the complex nonlinear relationship that arises in other methods developed for assimilating Lagrangian data in which the change in drifter position is used to provide an estimate

of the flow velocity. The observations $\mathbf{y}^o(t_k)$ can be expressed as

$$\mathbf{y}^o(t_k) = \mathbf{H}\mathbf{x}^t(t_k) + \boldsymbol{\epsilon}^t(t_k), \tag{11}$$

and $\boldsymbol{\epsilon}^t(t_k)$ are random variables representing measurement errors. We assume the errors to be uncorrelated zero-mean Gaussian with a covariance

$$E\{\boldsymbol{\epsilon}^t(t_k)[\boldsymbol{\epsilon}^t(t_l)]^{\mathrm{T}}\} = \delta_{kl}\mathbf{R}^t. \tag{12}$$

The additional error $\widetilde{\boldsymbol{\epsilon}_j^f}(t_k)$, introduced to each ensemble member in Eq. (8), is required to circumvent the problem of generating an updated ensemble that has a variance that is too low. Burgers et al. (1998) showed that the additional perturbations for the EnKF produces an approach that is entirely consistent with the standard Kalman filter since the covariance of the ensemble can be interpreted as the prediction error covariance. This additional error is added in a way that ensures it has zero mean and an uncorrelated Gaussian with variance given by

$$\frac{1}{N_E - 1}\sum_{j=1}^{N_E}[\widetilde{\boldsymbol{\epsilon}_j^f}(t_k)][\widetilde{\boldsymbol{\epsilon}_j^f}(t_l)]^{\mathrm{T}} = \delta_{kl}\mathbf{R}_e, \tag{13}$$

where $\mathbf{R}_e$ is an ensemble covariance matrix that converges to $\mathbf{R}$ of Eq. (12) in the limit $N_E \to \infty$. We point out that other approaches can be used to reproduce the covariances without having to perturb the observations. Such methods include the ensemble adjustment Kalman filter of Anderson (2001) and the ensemble transform Kalman filter of Bishop et al. (2001). With the above definitions, the analysis error covariance matrix corresponding to the updated ensemble members will be given by

$$\mathbf{P}_e^a = (\mathbf{I} - \mathbf{K}\mathbf{H})\mathbf{P}_e^f, \tag{14}$$

and is consistent with the form given by the EKF.

The augmented model approach that we have presented above for assimilating Lagrangian data has certain attractive properties that we can exploit to reduce the computational overhead in our implementation, which we shall now discuss. To clarify our arguments, we will write the covariance matrix for the augmented system in a block matrix form as

$$\mathbf{P}_e = \begin{bmatrix} (\mathbf{P}_{FF})_e & (\mathbf{P}_{FD})_e \\ (\mathbf{P}_{DF})_e & (\mathbf{P}_{DD})_e \end{bmatrix}, \tag{15}$$

where $(\mathbf{P}_{FF})_e$, $(\mathbf{P}_{FD})_e$, $(\mathbf{P}_{DF})_e$, and $(\mathbf{P}_{DD})_e$ are $(N \times N)$, $(N \times L)$, $(L \times N)$, and $(L \times L)$ matrices, respectively. We recall that N represents the size of the state vector of the dynamic model whereas L corresponds to the number of available observations. In practice, the number of available observations will be much less than the size of the state vector used to represent the model state, that is, $L \ll N$. In this case, the additional cost associated with integrating the augmented system will generally be a small fraction of the overall cost of the computation.

A direct consequence of the form of $\mathbf{H}$ that is obtained in our formulation is the special form of the Kalman gain matrix, which reduces to

$$\mathbf{K} = \begin{bmatrix} (\mathbf{P}_{FD})_e \\ (\mathbf{P}_{DD})_e \end{bmatrix}[(\mathbf{P}_{DD})_e + \mathbf{R}_e]^{-1}. \tag{16}$$

Only those elements of $\mathbf{P}_e$ appearing in Eq. (16) need to be computed in the EnKF. Recalling that in general $(\mathbf{P}_{FF})_e$ is computationally the most expensive part in constructing the covariance matrix since $N \gg L$, we note that the above simplification results in a substantial reduction in cost. Furthermore, we only need to invert an $L \times L$ matrix in Eq. (16), and together with the above savings produces a very efficient method for constructing the Kalman gain matrix. At this stage, it is important to emphasize that while the form of $\mathbf{K}$ will be identical in both the EKF and the EnKF formulation, the above simplifications cannot be fully exploited in the EKF. This arises from an implicit dependence of $\mathbf{K}$ on $(\mathbf{P}_{FF})_e$ through $(\mathbf{P}_{FD})_e$ and $(\mathbf{P}_{DD})_e$. Given that the covariance matrix is computed explicitly in the EKF, Kuznetsov et al. (2003) pointed out that an explicit computation of $(\mathbf{P}_{FF})_e$ is needed to obtain $(\mathbf{P}_{FD})_e$ and $(\mathbf{P}_{DD})_e$. In contrast, the EnKF permits us to take full advantage of the structure of the Kalman gain matrix, making it very appropriate to use together with our formulation for assimilating Lagrangian data.

The formulation presented above will generally work without any further modifications provided the ensemble size N_E is sufficiently large to provide accurate statistics for the error covariances associated with the system under consideration. In general, however, N_E will be restricted to $O(100)$. Under certain circumstances this finite ensemble size can degrade the performance of the filter at the assimilation step. Cohn and Parrish (1991) and Mitchell et al. (2002) have analyzed the problem and have noted that a small ensemble size produces noisy correlations between remote points within the flow. This in turn degraded the convergence of their filter. They tackled the problem by proposing a localization function with local support that retains correlations estimated by the ensemble within a local neighborhood but suppresses all correlations beyond a specified cutoff radius. We have encountered a similar problem in some of our simulations to be presented later. We therefore modify the definition of the Kalman gain matrix by introducing a localization matrix $\boldsymbol{\rho}$ such that

$$\mathbf{K} = \begin{bmatrix} \boldsymbol{\rho}_{FD} \circ (\mathbf{P}_{FD})_e \\ \boldsymbol{\rho}_{DD} \circ (\mathbf{P}_{DD})_e \end{bmatrix} [\boldsymbol{\rho}_{DD} \circ (\mathbf{P}_{DD})_e + \mathbf{R}_e]^{-1}. \quad (17)$$

Here $\boldsymbol{\rho}_{FD}$ is an $N \times L$ matrix and $\boldsymbol{\rho}_{DD}$ is an $L \times L$ matrix. The operator $\circ$ denotes the Schur product of two matrices. The elements of $\boldsymbol{\rho}$ correspond to a distance-dependent cutoff function. In this work, we employ a smooth cutoff function and have chosen to use the form given by Hamill et al. (2001). In Lagrangian data assimilation, both $\boldsymbol{\rho}_{FD}$ and $\boldsymbol{\rho}_{DD}$ are time-dependent matrices since the localization is a function of the changing drifter positions. The localization matrices are, therefore, computed at each assimilation step. In constructing these matrices, we have used the drifter positions at the assimilation step to compute the localization functions although other alternatives may be possible (e.g., intermediate positions taken between consecutive assimilation steps).

3. Mathematical model and experimental setup

a. Flow model

We consider an idealized ocean model with a square domain configuration whose size in the zonal and meridional directions is denoted by L_x and L_y, respectively. As described in Cushman-Roisin (1994) and Pedlosky (1987), the flow within this domain can be modeled by the reduced-gravity shallow-water system of equations, which are given by

$$\frac{\partial h}{\partial t} = -\frac{\partial (hu)}{\partial x} - \frac{\partial (h\upsilon)}{\partial y}, \quad (18)$$

$$\frac{\partial u}{\partial t} = -u\frac{\partial u}{\partial x} - \upsilon\frac{\partial u}{\partial y} + f\upsilon - g'\frac{\partial h}{\partial x} + F^u + \nu\nabla^2 u, \quad (19)$$

$$\frac{\partial \upsilon}{\partial t} = -u\frac{\partial \upsilon}{\partial x} - \upsilon\frac{\partial \upsilon}{\partial y} - fu - g'\frac{\partial h}{\partial y} + \nu\nabla^2 \upsilon, \quad (20)$$

with the boundary and initial conditions given by

$$u(x, y, t)|_{\partial\Omega} = 0, \quad \upsilon(x, y, t)|_{\partial\Omega} = 0, \quad (21)$$

$$u(x, y, 0) = 0, \quad \upsilon(x, y, 0) = 0, \quad h(x, y, 0) = H_o, \quad (22)$$

where $\partial\Omega$ represents the boundaries of our flow domain, h is the surface height, (u, υ) is the fluid-velocity vector, g' is the reduced gravity, υ is interpreted as a (constant) eddy viscosity, F^u is a horizontal wind forcing acting in the zonal direction, and f is the Coriolis parameter. We invoke the β-plane approximation allowing the Coriolis term to be expressed as

$$f = f_o + \beta y, \quad (23)$$

where f_o and β are constants. A zonal wind forcing of the form

TABLE 1. Parameters fixed for reduced-gravity shallow-water equations.

Property	Value
L_x	2000 km
L_υ	2000 km
f_o	6×10^{-5} s^{-1}
β	2×10^{-11} m^{-1} s^{-1}
H_o	500 m
g'	0.02 m s^{-2}
ρ	1000 kg m^{-3}
τ_o	0.05 N m^{-2}
Δx	20 km
Δy	20 km
Δt	12 min

$$F^u = \frac{-\tau_o}{\rho H_o(t)} \cos(2\pi y/L_y), \quad (24)$$

$$H_o(t) = \frac{1}{L_x L_y} \int_0^{L_x} \int_0^{L_y} h(x, y, t)\, dx\, dy, \quad (25)$$

is employed in this work, where x and y are the coordinates in the zonal and meridional directions measured from the western and southern boundaries of our flow domain, respectively, τ_o is the wind stress, ρ is the density of water, and $H_o(t)$ the average water depth. We note that in general, $H_o(t)$ is a quantity that is conserved by our system of equations. The parameter $H_o(t) = H_o(0)$ is, therefore, a parameter that is prescribed by our initial conditions. This is not generally true at assimilation steps in which the average water depth may change. By retaining the time dependence in Eq. (24), we can make sure that the physical wind stress acting on our system is unaltered at assimilation steps. To solve the model described above, we assigned the parameters given in Table 1. With these flow conditions, the wind forcing drives a double-gyre circulation with the familiar dynamics of Sverdrup gyres, western boundary currents, midlatitude jet, and mesoscale eddies. The extensive and widespread studies that have covered this specific setup in the oceanographic community make it an ideal model to demonstrate our data assimilation methods.

In addition to the above equations governing the evolution of the flow dynamics, we model drifters/floats deployed for measurements of the ocean as passive Lagrangian tracers. Under this assumption, the drifters move with the local fluid velocity vector and are governed by the equations

$$\frac{d\mathbf{x}_D(t)}{dt} = u[\mathbf{x}_D(t), \mathbf{y}_D(t), t], \quad (26)$$

$$\frac{d\mathbf{y}_D(t)}{dt} = \upsilon[\mathbf{x}_D(t), \mathbf{y}_D(t), t], \quad (27)$$

with the initial conditions

$$\mathbf{x}_D(0) = \boldsymbol{\alpha} \quad \mathbf{y}_D(0) = \boldsymbol{\beta}. \tag{28}$$

Here $\mathbf{x}_D$ and $\mathbf{y}_D$ are both vectors of dimension $\mathbf{N}_D$ and represent the positions of the drifters in our flow domain.

The flow, together with the drifter equations given above, comprises the augmented system referred to in section 2. To cast our model into the forms given by Eqs. (1) and (2), we discretize our flow equations on an $(n_x \times n_y) = (100 \times 100)$ grid such that each cell size is given by $(\Delta x, \Delta y) = (20 \text{ km}, 20 \text{ km})$. This spatial discretization produces a set of N ordinary differential equations with $N = 2(n_x - 1)(n_y - 1) + n_x n_y$ (velocity vectors are stored at cell nodes whereas the height field is stored at cell centers). The flow state vector x_F is then given by $\mathbf{x}_F(t) = [u_{1,1}(t), \cdots, u_{n_x-1,n_y-1}(t), v_{1,1}(t), \cdots, v_{n_x-1,n_y-1}(t), h_{1,1}(t), \cdots, h_{n_x,n_y}(t)]$. The $\mathbf{m}_F$ operator appearing in Eq. (1) then corresponds to the discretized form of the terms on the right-hand side of Eqs. (18)–(20). The operator $\mathbf{m}_D$ of Eq. (2) can be related directly to the system of Eqs. (26)–(27), which represent a set of ordinary differential equations for the N_D drifters. We note that to avoid velocities that violate our no-slip/no-normal flow boundary conditions, we do not include velocity data at our domain boundaries in our flow state vector $(\mathbf{x}_F)$ at the assimilation step.

b. Twin-experiment setup

In this study, we will employ the twin-experiment setup in which the same flow and drifter equations are used to provide both the model forecast $\mathbf{x}^f$ and the "true" state $\mathbf{x}^t$. The advantage of this approach is that appropriate performance metrics can be defined, which allows us to establish how well our method can reconstruct the flow state space $\mathbf{x}_F^f$ of our model by observing only drifter positions $\mathbf{x}_D^t$ from the true system. To produce two different sets of flows from our shallow-water equations, we employ a different initial condition for the averaged water depth H_o in the two systems. This choice is motivated by the realization that H_o is a conserved quantity that remains constant without the assimilation of data. This provides an ideal benchmark problem in which we can test whether our method can recover the true value of H_o by simply propagating the information from the drifter measurements through the error covariance matrix to correct the height field. This approach is in contrast to that of Özgökmen et al. (2003) who used identical parameters for both the forecast and the true systems. The difference between the two systems in their case was then introduced by integrating the true flow model until a statistically stationary flow was established whereas the model forecast was simulated from rest. Another distinctive feature between our method and that of Özgökmen et al. is that our height field forms a subset of the state vector to be corrected at assimilation steps. This allows the average water depth to be adjusted directly by the method, providing an approach to recover the correct value of H_o. The algorithm of Özgökmen et al., on the other hand, only corrects the velocity field from observed drifter data. The height field is then adjusted in their computations by employing a dynamic condition based on the assumption of geostrophic balance. This yields a Poisson-type equation to correct the height field, raising further complications in the assimilation of data into primitive equation models. No such specific treatments are required with our approach, producing a relatively simpler approach to correct the prognostic flow variables in our model.

For the computations that we will present in the following section, we have set $H_o = 500$ m for the true system and considered a 10% error in the mean value of the model (the mean over our ensemble was set to $H_o = 550$ m). A Gaussian distribution with a variance of $\sigma_h = 50$ m was used to generate H_o for the different members of our ensemble. To integrate the equations for the two systems, we used standard central differencing for the momentum equations [(19)–(20)] and a multidimensional positive definite advection transport algorithm (MPDATA) scheme (Smolarkiewicz and Margolin 1998) for the continuity equation [(18)]. We initially integrated the systems for a period of 12 yr with a time step of $\Delta t = 12$ min to establish a statistically steady state. This initial run produces a distinct velocity and height field for the true flow and each ensemble member of our model forecast. At the end of the 12th year, drifters are released into the true system. Each drifter is initialized at a specified location within the flow domain with the observation errors taken to be distributed as independent Gaussians with the same statistics; that is,

$$E[\boldsymbol{\epsilon}^{(x)}(t_k)\boldsymbol{\epsilon}^{(x)}(t_l)] = E[\boldsymbol{\epsilon}^{(y)}(t_k)\boldsymbol{\epsilon}^{(y)}(t_l)] = \delta_{kl}\sigma^2\mathbf{I},$$
$$E[\boldsymbol{\epsilon}^{(x)}(t_k)] = E[\boldsymbol{\epsilon}^{(y)}(t_k)] = E[\boldsymbol{\epsilon}^{(x)}(t_k)\boldsymbol{\epsilon}^{(y)}(t_l)] = 0, \tag{29}$$

where σ is taken to be 200 m in this work. These perturbed drifters are then integrated with our true flow over a period of 1 yr to generate a set of true trajectories. Each ensemble member of our forecast model is then integrated over the same 1-yr time interval using a corresponding set of perturbed drifters with the same error statistics as those given in Eq. (29). At assimilation steps, only drifter locations from the true system are assimilated into the model at specified time intervals. The specific number of drifters, their release location, assimilation time interval, as well as the number of

TABLE 2. Parameters varied in our numerical simulations.

Experiment	Viscosity ($m^2\ s^{-1}$)	Localization radius (km)	No. of members	No. of drifters	Drifter release location	Assimilation time step (days)
1	500	No localization	80	1	A	1
2	400	No localization	80	1	A	1
3	400	No localization	80	36	C	1
4	400	300, 600, 1200	80	36	C	1
5	400	300, 600	20, 40, 80	36	C	1
6	400	600	80	36	C	1–20
7	400	600	80	4–64	C	1
8	400	600	80	16, 21	A, B, C	1

ensemble members, are varied throughout our numerical experiments to identify the sensitivity of our scheme on these parameters. The range of values and type of experiments considered and discussed in the following section are given in Table 2. For simplicity, we will refer to the region $[(x, y)|0\ \text{km} < x < 700\ \text{km}, 700\ \text{km} < y < 1300\ \text{km}]$ as region A, the region $[(x, y)|1300\ \text{km} < x < 2000\ \text{km}, 0\ \text{km} < y < 700\ \text{km}]$ as region B, and the entire flow domain $[(x, y)|0\ \text{km} < x < 2000\ \text{km}, 0\ \text{km} < y < 2000\ \text{km}]$ as region C.

To quantify the performance of the method, we introduce several different norms that are used extensively in our subsequent discussions. These provide a measure of the errors in our velocity field, height field, and drifter locations. The true errors for the kinetic energy, height field, and drifter separation distances are given by

$$|\mathrm{KE}|^{\mathrm{t}} = \sqrt{\frac{\sum_{i=1}^{n_x-1}\sum_{j=1}^{n_y-1}(\overline{u^f_{i,j}} - u^t_{i,j})^2 + (\overline{v^f_{i,j}} - v^t_{i,j})^2}{\sum_{i=1}^{n_x-1}\sum_{j=1}^{n_y-1}(u^t_{i,j})^2 + (v^t_{i,j})^2}}, \tag{30}$$

$$|\mathrm{h}|^{\mathrm{t}} = \sqrt{\frac{\sum_{i=1}^{n_x}\sum_{j=1}^{n_y}(\overline{h^f_{i,j}} - h^t_{i,j})^2}{\sum_{i=1}^{n_x}\sum_{j=1}^{n_y}(h^t_{i,j})^2}}, \tag{31}$$

$$|\mathbf{x}_D|^t = \frac{1}{\sigma}\sqrt{\frac{\sum_{i=1}^{N_D}(\overline{x^f_{D,i}} - x^t_{D,i})^2 + (\overline{y^f_{D,i}} - y^t_{D,i})^2}{N_D}}, \tag{32}$$

$$\overline{u^f_{i,j}} = \frac{1}{N_E}\sum_{k=1}^{N_E}(u_k)_{i,j}, \quad \overline{v^f_{i,j}} = \frac{1}{N_E}\sum_{k=1}^{N_E}(v_k)_{i,j},$$

$$\overline{h^f_{i,j}} = \frac{1}{N_E}\sum_{k=1}^{N_E}(h_k)_{i,j}, \tag{33}$$

$$\overline{x^f_{D,i}} = \frac{1}{N_E}\sum_{k=1}^{N_E}(x_D)_{k,i}, \quad \overline{y^f_{D,i}} = \frac{1}{N_E}\sum_{k=1}^{N_E}(y_D)_{k,i}, \tag{34}$$

respectively. The predicted errors, as computed by our ensemble Kalman filter are given by

$$|\mathrm{KE}|^{\mathrm{p}} = \sqrt{\frac{\left[\sum_{k=1}^{N_E}\sum_{i=1}^{n_x-1}\sum_{j=1}^{n_y-1}(\overline{u^f_{i,j}} - (u^j_k)_{i,j})^2 + (\overline{v^f_{i,j}} - (v^f_k)_{i,j})^2\right]/(N_E - 1)}{\sum_{i=1}^{n_x-1}\sum_{j=1}^{n_y-1}(\overline{u^f_{i,j}})^2 + (\overline{v^f_{i,j}})^2}}, \tag{35}$$

$$|\mathrm{h}|^{\mathrm{p}} = \sqrt{\frac{\left\{\sum_{k=1}^{N_E}\sum_{i=1}^{n_x}\sum_{j=1}^{n_y}[\overline{h^f_{i,j}} - (h^f_k)_{i,j}]^2\right\}/(N_E - 1)}{\sum_{i=1}^{n_x}\sum_{j=1}^{n_y}(\overline{h^f_{i,j}})^2}}, \tag{36}$$

$$|\mathbf{x}_D|^p = \frac{1}{\sigma}\sqrt{\frac{\sum_{k=1}^{N_E}\sum_{i=1}^{N_D}[\overline{x^f_{D,i}} - (x^f_D)_{k,i}]^2 + [\overline{y^f_{D,i}} - (y^f_D)_{k,i}]^2}{N_D(N_E - 1)}}. \tag{37}$$

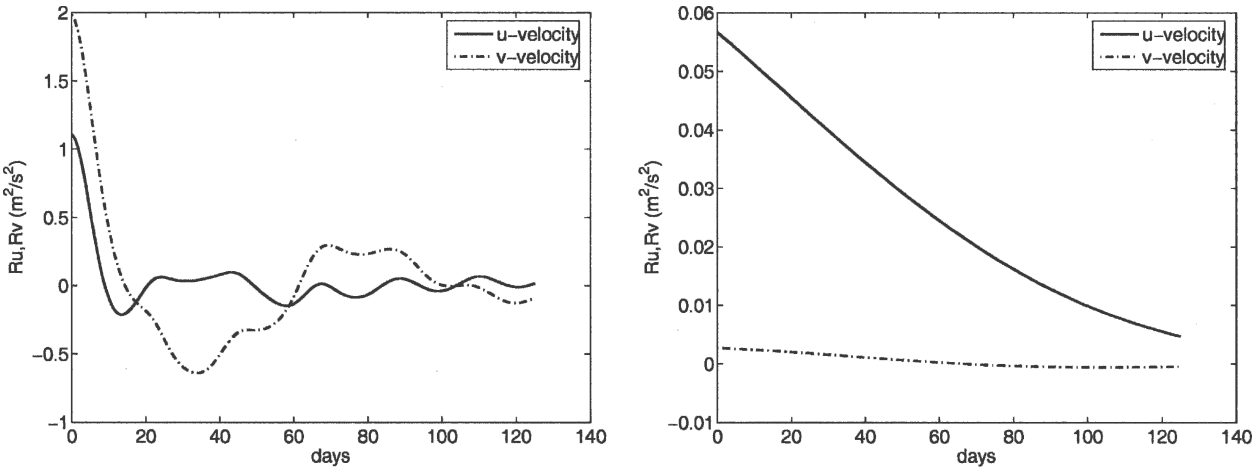

(a) Within the mid-latitude jet region. **(b) Within the quiescent part of the lower gyre.**

FIG. 1. Lagrangian autocorrelation function.

4. Results

a. Benchmark flow

We begin with a detailed analysis of our results for the benchmark experiment (number 1) listed in Table 1. In this experiment, we have set the assimilation time step to 1 day. The success of the assimilation will inevitably depend on how this time scale relates to the flow time scales in our flow (see Molcard et al. 2003). Given that the focus is on the use of Lagrangian data, we have computed the Lagrangian autocorrelation time scale for the true flow by releasing a set of 6×6 drifters in the turbulent region of the flow (region A) and also in the quiescent region (region B). Autocorrelation functions for the u and v components of velocity and denoted by Ru and Rv, respectively, were computed and are presented in Fig. 1 for both regions. The initial rapid decay seen in Fig. 1a is a reflection of the shorter Lagrangian time scales (T_L) that are found in this part of the flow. This is in stark contrast to the Lagrangian time scales associated with region B, which are much longer as reflected in Fig. 1b. If we define the Lagrangian time scale as the time it takes for the autocorrelation function to first intersect the x axis, then we can conclude from Fig. 1a that $T_L \approx 10$–15 days in our simulations. In fact, the results do not vary significantly by reducing the viscosity to $\nu = 400$ m^2 s^{-1}. We can therefore take this value of T_L as typical of the simulations that we consider throughout this section. The 1-day assimilation time step we have chosen is, therefore, around 10% of T_L, and we can be confident that our assimilation frequency is sufficiently high for this particular flow regime. To test the scheme, we have assimilated a single drifter trajectory released in region A ($x_D = 600$ km, $y_D = 1000$ km). This particular release site was motivated by the findings of Kuznetsov et al. (2003) and Molcard et al. (2003) who identified the importance of sampling the complex spatiotemporal structure of the flow for the assimilation to be successful.

Initially, we assess the performance of the method using qualitative measures in terms of the spatial distributions of the height and vorticity fields. Results for the height–perturbation field ($h - H_o$) are given in Fig. 2 at three different times corresponding to 0 days (measured from the beginning of the assimilation cycle, i.e., year 12), 30 days, and 90 days. Three different sets of plots are included, the first for the true flow, the second for the assimilated flow, and the third for a model run without assimilation. Results for the model runs are based on the mean of the ensemble. At 0 days, we note that the true height field differs from the other two flows, which are identical. After 30 days, during which 30 assimilation steps have been performed, the assimilated case now resembles the true flow more closely with some localized differences. In contrast, the nonassimilated case shows fewer negative isocontours in similarity to Fig. 2a(iii) and is associated with the higher water depth we used to initialize the model runs. By 90 days, we observe essentially identical contours between the true and assimilated systems, which by now are significantly different from the nonassimilated flow. This is clearly depicted in the pinched-off eddy that is seen in Figs. 2c(i) and 2c(ii), but does not appear in Fig. 2c(iii). An analysis of the vorticity field presented in Fig. 3 reveals a very similar evolution of the three different flows. Initially, both Figs. 3a(ii) and 3a(iii) are identical and distinct from Fig. 3a(i). However, as as-

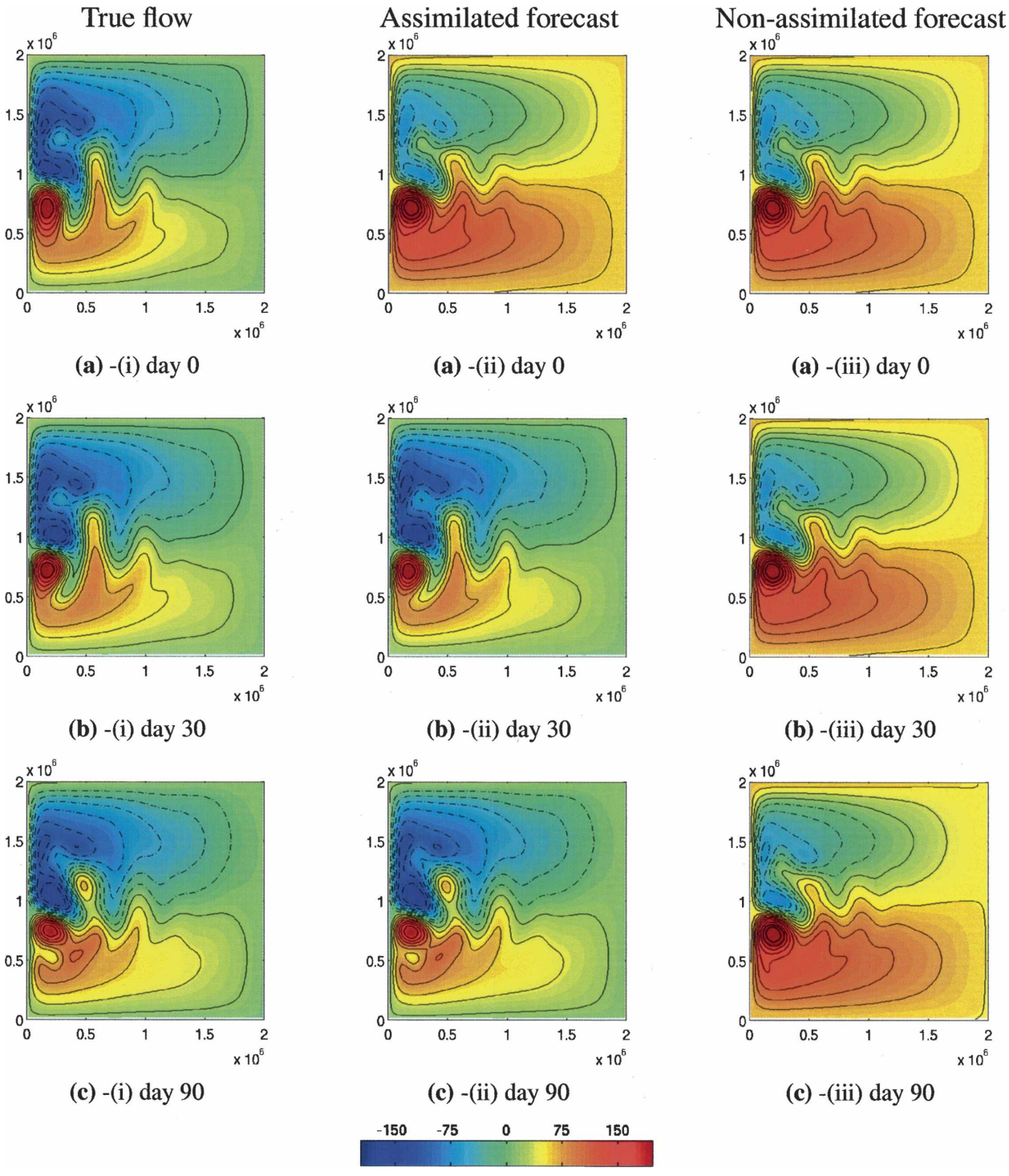

FIG. 2. Isocontours of height perturbation (h–H_o) shown at three different times measured from the beginning of the assimilation interval. The three sets of flows correspond to the true target flow, the assimilated forecast, and the nonassimilated forecast.

similation is performed, the assimilated system gradually evolves to produce flow structures that closely mimic those in the true system. By 90 days both the assimilated and true flows are essentially identical. The nonassimilated flow, on the other hand, exhibits a vorticity field that is very different, which is consistent with the results presented for the height field.

To provide a more quantitative measure of the con-

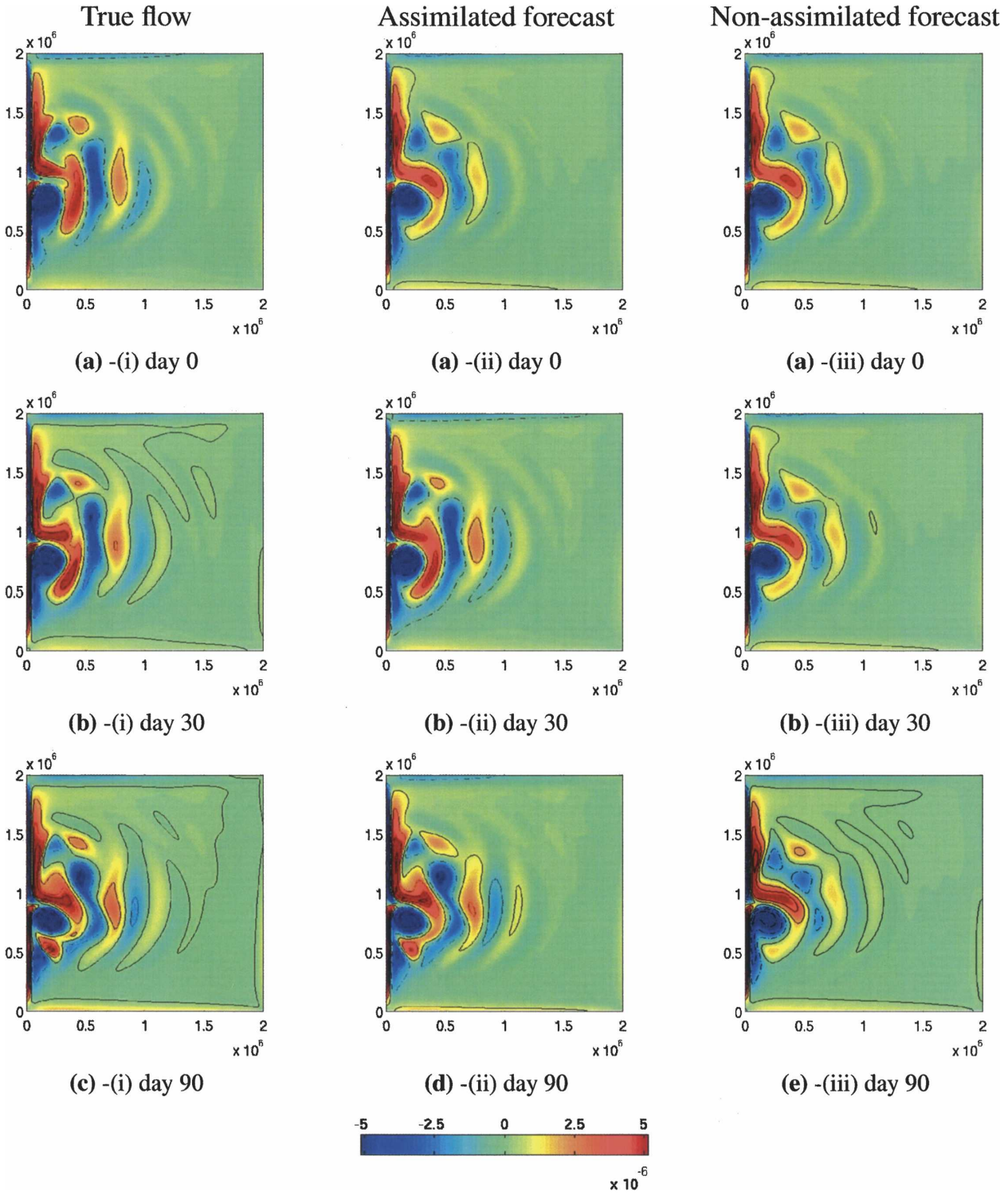

FIG. 3. Isocontours of dynamic vorticity field shown at three different times measured from the beginning of the assimilation interval. The three sets of flows correspond to the true target flow, the assimilated forecast, and the nonassimilated forecast.

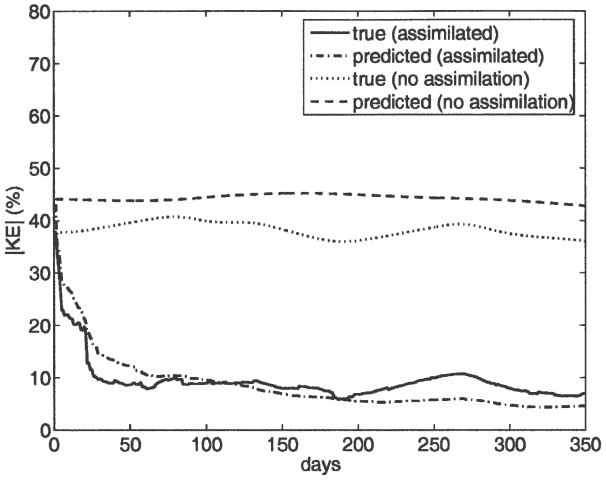

(a) Error in kinetic energy.

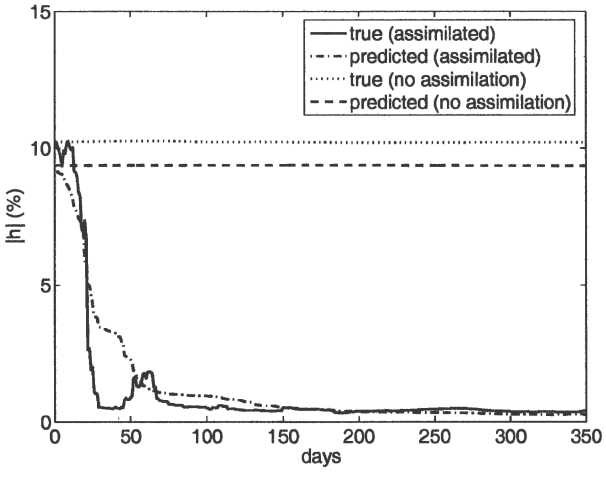

(b) Error in height field.

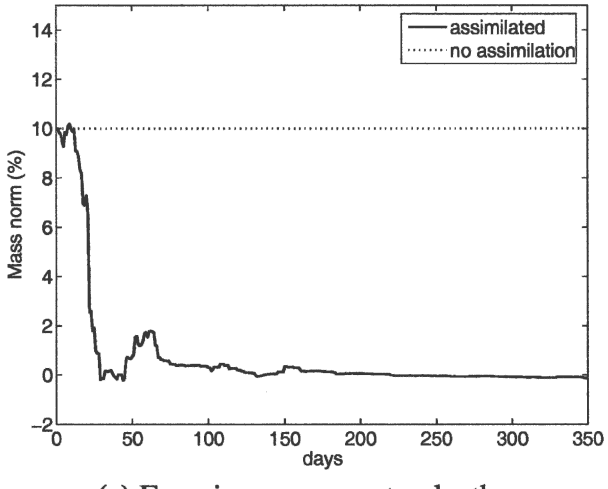

(c) Error in average water depth.

FIG. 4. Flow error convergence corresponding to expt 1; $\nu = 500$ m^2 s^{-1} and using one drifter with an assimilation time step of 1 day.

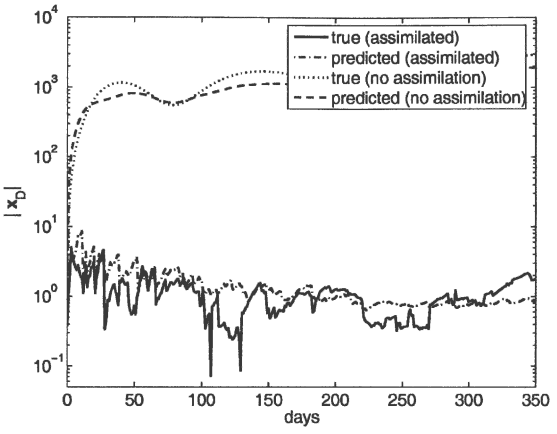

(a) Error in drifter position.

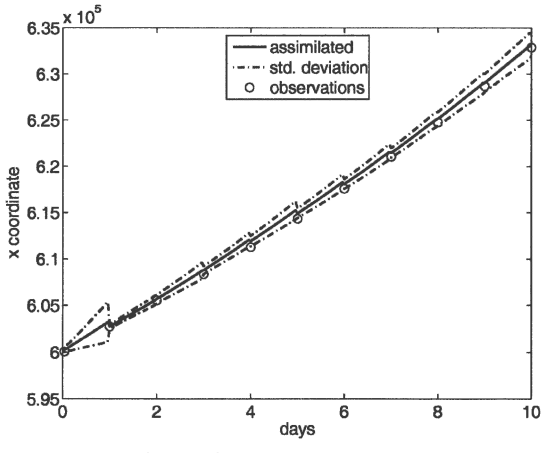

(b) Zonal coordinate of drifter position.

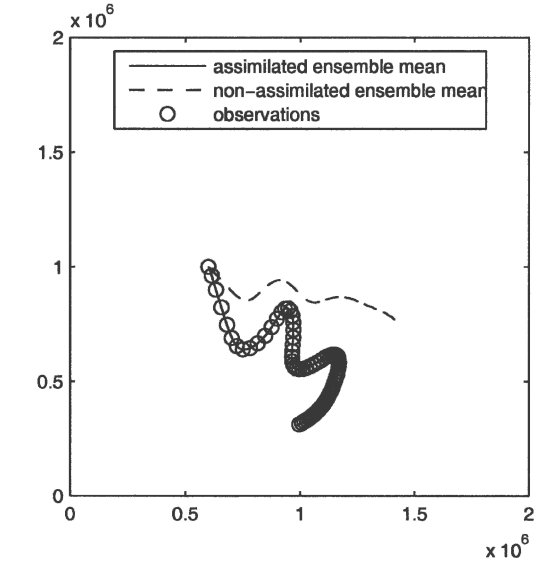

(c) Drifter trajectories.

FIG. 5. Drifter error convergence corresponding to expt 1; $\nu = 500$ m^2 s^{-1} and using one drifter with an assimilation time step of 1 day.

vergence of our assimilation experiment, we have computed the error norms defined in section 3b. Error norms associated with the flow field are shown in Fig. 4 in terms of the kinetic energy, height field, and height-averaged water depth as functions of time. For purposes of comparison, we have also included the case without assimilation to reflect the relative improvement in assimilating the drifter data. We note that within a time scale of around 60 days, the error has almost been eliminated from our system with assimilation. Another striking feature is that, while the predicted error exhibits an essentially monotonic reduction (since this is the error that the EnKF reduces), the true error is oscillatory by comparison. Despite these discrepancies, both errors have essentially the same time history, a feature that is necessary for the EnKF to successfully drive down the true error. This implies that the error statistics for this particular experiment are well represented by our ensemble.

Error norms for the drifter position are shown in Fig. 5a on a log–log scale. In similarity to the errors for the flow, we note that both predicted and true errors in the assimilated run are of the order of the error variance used in our Kalman filter, indicating successful tracking of the drifter trajectories. Without assimilation, the drifters show an exponentially rapid divergence from the true drifter trajectory. This behavior is characteristic of the presence of Lagrangian saddle points that in the presence of unsteady dynamics produce chaotic Lagrangian motion and exponential separation of nearby trajectories. Such a behavior can be attributed to positive Lyapunov exponents in the flow (see Aref and El Naschie 1995 for a detailed review). To illustrate how our method successfully tracks the true drifter trajectory, Fig. 5b shows the assimilated x coordinate of our drifter together with the standard deviation given by our ensemble, and the observed drifter position at 1-day intervals. The figure demonstrates how the assimilated trajectory is updated at each day to retain the error with respect to the true drifter position within the error tolerance represented by the standard deviation. In contrast, the nonassimilated trajectory and the associated error both diverge very rapidly as alluded to in Fig. 5a. Figure 5c illustrates the trajectories taken by the drifter in the assimilated and nonassimilated systems together with the true drifter trajectory. The figure clearly illustrates the successful tracking of the true trajectory in the assimilated model.

The results presented above demonstrate the success of the method in assimilating Lagrangian data. However, given that a single drifter was used to correct the entire flow, a natural question to pose is, Can the method work for flows with more complex flow dynamics whereby more than a single drifter is needed? To generate such a flow we lower the (eddy) viscosity to $\nu = 400\ \mathrm{m}^2\ \mathrm{s}^{-1}$. After repeating our simulations for this case (experiment 2), we computed the respective flow and drifter norms, and these are shown in Fig. 6. Focusing on the results for the single drifter, we observe a more erratic signature in the true errors for both the kinetic energy and the height fields. The errors appear to converge more slowly relative to experiment 1. In stark contrast, the predicted errors show a gradual and smooth decay toward zero, deviating substantially from the true errors. Analyzing the drifter norms also appears to indicate an inability to track the drifter for longer times (beyond 250 days). Our first attempt to rectify this problem was to assimilate more drifter locations under the expectation that more data are needed for this dynamically more active flow. After repeating our experiment with 36 drifters uniformly distributed within the domain, we found that the true flow errors did not improve significantly as seen from Figs. 6a and 6b. In the case of the true drifter norm, the true error was seen to deviate more rapidly than in the case with one drifter (Fig. 6c). The predicted errors on the other hand all showed a rapid decrease within the first few days and were lower than the levels obtained with one drifter. This anomalous behavior in the predicted error arises in the EnKF when the ensemble size is not large enough to provide statistically accurate error covariances. Consequently, the EnKF continues to update the system based on the behavior of the predicted error, which, as can be seen from our results, is almost completely unrelated to the true errors. An analysis of the problem of small ensemble size on the performance of the EnKF was conducted by Hamill et al. (2001) and Mitchell et al. (2002). To tackle this problem, they proposed to employ localization matrices of the form presented in section 2 to suppress the noisy correlations that arise for remote points in the system. Such an approach is common and was also employed in the work of Houtekamer and Mitchell (1998, 2001). We will therefore study whether our formulation with localization can resolve the problems outlined above with our Lagrangian data assimilation method.

b. Localization

The results presented in Fig. 7 correspond to experiment 4 of Table 2. Four sets of results are presented that reflect the effect that different localization radii have on the filter's performance. The case with no localization presented earlier in Fig. 6 for 36 drifters is also included for purposes of comparison. Given that we are primarily interested in driving the true error down, only true errors are presented in the figures.

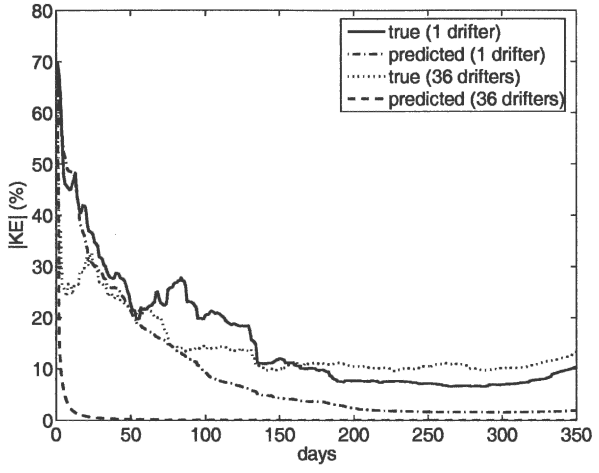

(a) Error in kinetic energy.

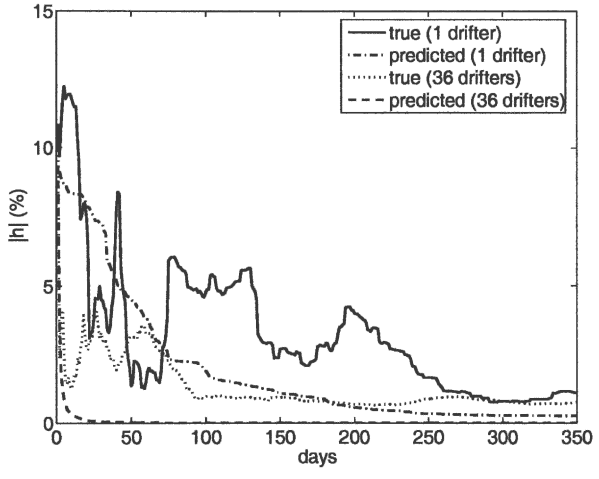

(b) Error in height field.

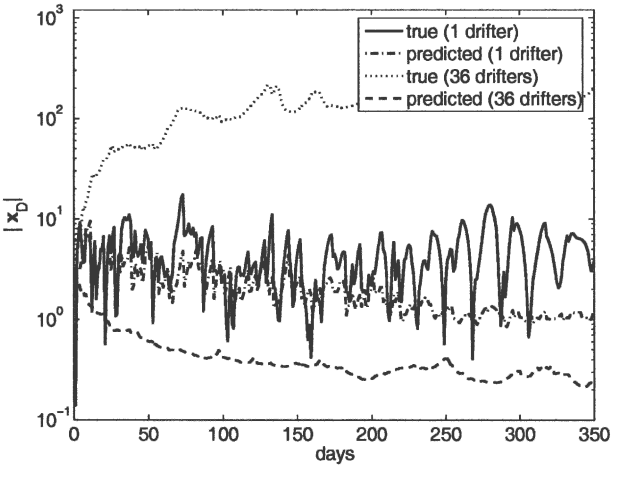

(c) Error in drifter positions.

FIG. 6. Flow/drifter error convergence corresponding to expts 2 and 3; $\nu = 400$ m^2 s^{-1} and using 1 and 36 drifters with an assimilation time step of 1 day.

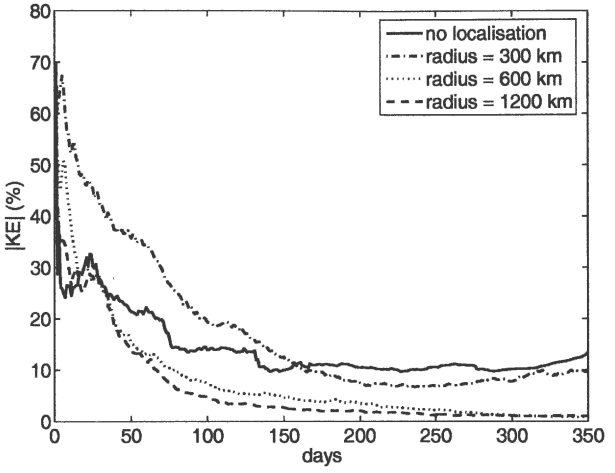

(a) Error in kinetic energy.

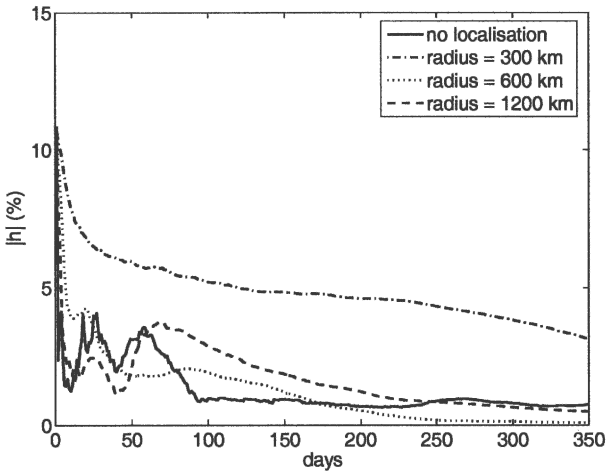

(b) Error in height field.

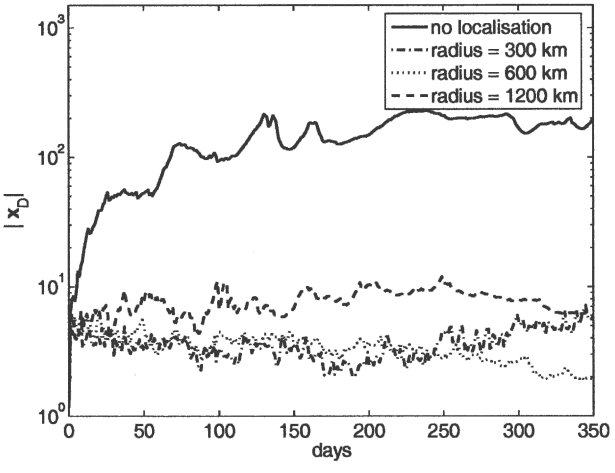

(c) Error in drifter positions.

FIG. 7. Influence of localization on error convergence for expt 4; $\nu = 400$ m^2 s^{-1} and using 36 drifters with an assimilation time step of 1 day.

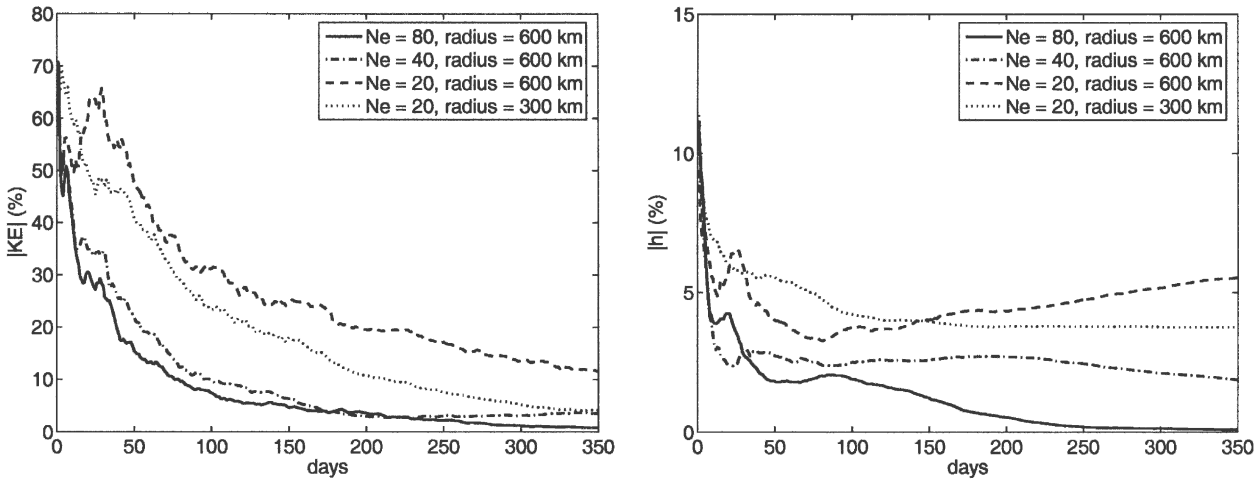

(a) Error in kinetic energy. (b) Error in height field.

FIG. 8. Influence of ensemble size on error convergence for expt 5.

Comparison of the results with and without localization clearly reveals a smoother decay in the error for both the kinetic energy and height fields as presented in Figs. 7a and 7b, respectively. The most significant improvement, however, is realized in the tracking of the drifter locations where all simulations performed with localization reveal a much smaller error relative to the case without localization. Closer inspection of the results indicates that a localization radius of 300 km results in the slowest decay such that an error of 10% and 4% remains in the kinetic energy and height fields at the end of 350 days, respectively. In comparison, a localization radius of 600 and 1200 km leads to a more rapid correction of the error within the first 50 days. Thereafter, the error continues to decrease and is essentially eliminated after 1 yr. Despite the stronger similarity in the results for $r_{\text{loc}} = 600$ km and $r_{\text{loc}} = 1200$ km, a localization radius of 600 km appears to be the optimum of the three values chosen for our flow. Inspection of the drifter errors confirms these observations.

The results presented here support our conjecture that the failure of the method to converge for experiments 2 and 3 was related to the use of a finite ensemble and the associated noisy correlations that arise. By localizing the covariance matrices, noisy correlations are eliminated, leading to a better performance of the EnKF. However, localization completely eliminates correlations between remote points, even those that are not deteriorated by the use of a small ensemble. Our ability to correct the flow with a small set of drifters is, therefore, diminished as the localization distance is reduced. More drifters will be needed to correct the flow in this case. Consequently, an optimum radius must be selected that eliminates the noisy correlations but retains the well-represented parts of the covariance matrix over the largest distance possible. In general, this optimum value is dependent on many parameters including the specific flow being modeled. Similar issues have been discussed by Houtekamer and Mitchell (1998, 2001) for Eulerian measurements. Having established the optimum value to be given by $r_{\text{loc}} = 600$ km, we will use this in the simulations that follow.

c. *Effect of ensemble size*

The importance of a finite ensemble size on our numerical simulations was clearly demonstrated in the preceding discussion. An important parameter to consider in our algorithm is, therefore, the sensitivity of the results to the size of the ensemble. In experiment 5, we have performed four additional simulations in which the size of the ensemble is varied. The results are presented in Fig. 8 in terms of the errors for the kinetic energy and the height field. By using the optimum value of $r_{\text{loc}} = 600$ km and systematically halving the size of our ensemble from 80 to 40, and finally to 20 members, a gradual degradation in the performance of the filter is observed. The most striking change in the kinetic energy occurs when we reduce N_E down to only 20 members. In this case, the error cannot be fully corrected within the 1-yr assimilation period. Contrasting these trends with results for the height field reveals a more sensitive dependence in the latter with respect to the size of the ensemble. In fact, by reducing N_E from 80 to 40 members, a saturation in the decay of the error for the height field is predicted. Further reduction of N_E to 20 hampers the convergence of the scheme, lead-

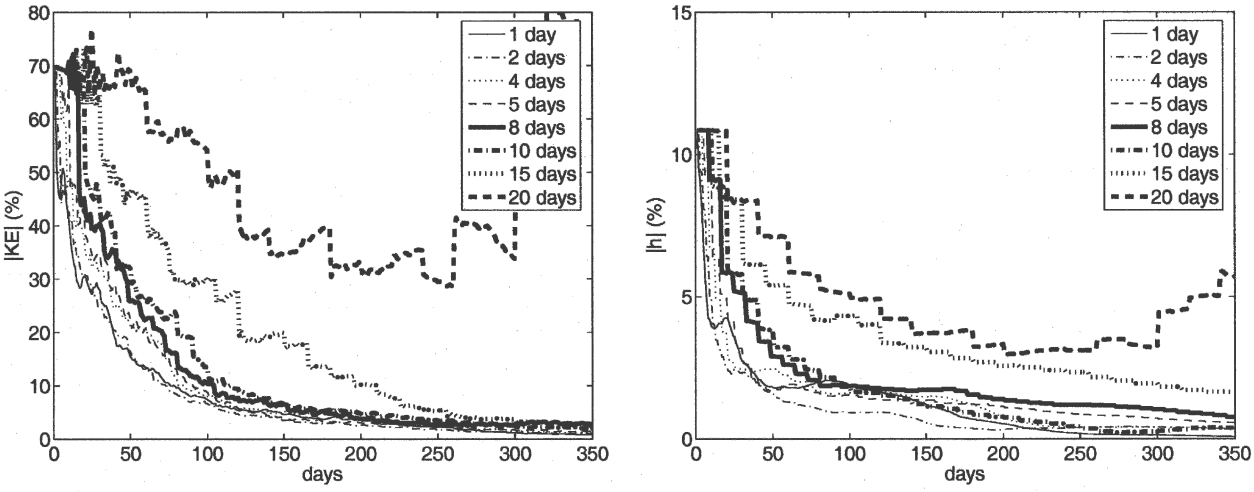

(a) Error in kinetic energy. (b) Error in height field.

FIG. 9. Influence of assimilation frequency on error convergence for expt 6.

ing to an eventual growth in the error for later times as seen in Fig. 8b.

The poor convergence observed for a small ensemble size is directly related to the noisy correlations we discussed above. We noted that for a given problem and size of ensemble, an optimum cutoff radius exists for our problem. As N_E is reduced, the optimum cutoff radius will also decrease. We expect the results for $N_E = 20$ to improve if we set a smaller value of r_{loc}. To verify this, we have repeated the simulation with $N_E = 20$ with a smaller value of the cutoff radius. Although this would allow a smaller region of the flow to be updated at assimilation steps, the results nevertheless indicate a clear improvement in the convergence of the method relative to the case $N_E = 20$, and $r_{\text{loc}} = 600$ km. This further confirms the detrimental impact of noisy correlations and demonstrates the dependence of the optimal cutoff radius on the size of our ensemble.

The parameters we have focused on thus far have been motivated by the observation that a small ensemble for the EnKF can lead to inaccurate estimation of the covariance matrix. Having uncovered the underlying issues arising from the use of a finite ensemble, a look at the influence of several key physical parameters will now be discussed. These parameters are important given the practical limitations set on the distribution of measurement instruments and the collection of their data. Examples include the rate at which data are sampled from our measurement instruments, the number of measurement sites available, and the spatial coverage of these instruments among a number of other parameters. Below we will focus on the influence of these physical parameters on the performance of our Lagrangian data assimilation method.

d. Assimilation frequency

An important physical parameter to consider is the frequency at which data are assimilated into our model. The realization that data may be sparsely scattered at given time intervals in our forecast raises the need to have a robust method that retains the convergence properties presented above for smaller assimilation frequencies (or longer assimilation time steps). To test the sensitivity of our augmented model approach to the assimilation frequency, we simulated a number of flows in which data were assimilated into the model over a range of time intervals. Results for the variation of the flow errors are presented in Figs. 9a and 9b. We note that for assimilation intervals of 1–10 days, our method remains insensitive to the specific interval used. Neither the initial rate of convergence nor the asymptotic values of the error at convergence change significantly. However, increasing the assimilation interval beyond 10 to 15 days shows the first sign of degradation in the convergence of the method. Increasing even further up to 20 days ultimately leads to failure of the method as seen by the increasing error levels beyond 250 days.

To clarify the nature of the failure observed for an assimilation time interval of 20 days, we analyze the drifter trajectories over the period [220, 280] of days spanning the time where the first sign of divergence in the flow appears. After analyzing all 36 drifters within the flow, we have identified 3 drifters that we can attribute to the divergence of the method. As would be expected, all three drifters are located near the western boundary of the domain in the vicinity of the midlatitude jet where the complex flow dynamics are realized. Figure 10 shows the trajectories of the three drifters.

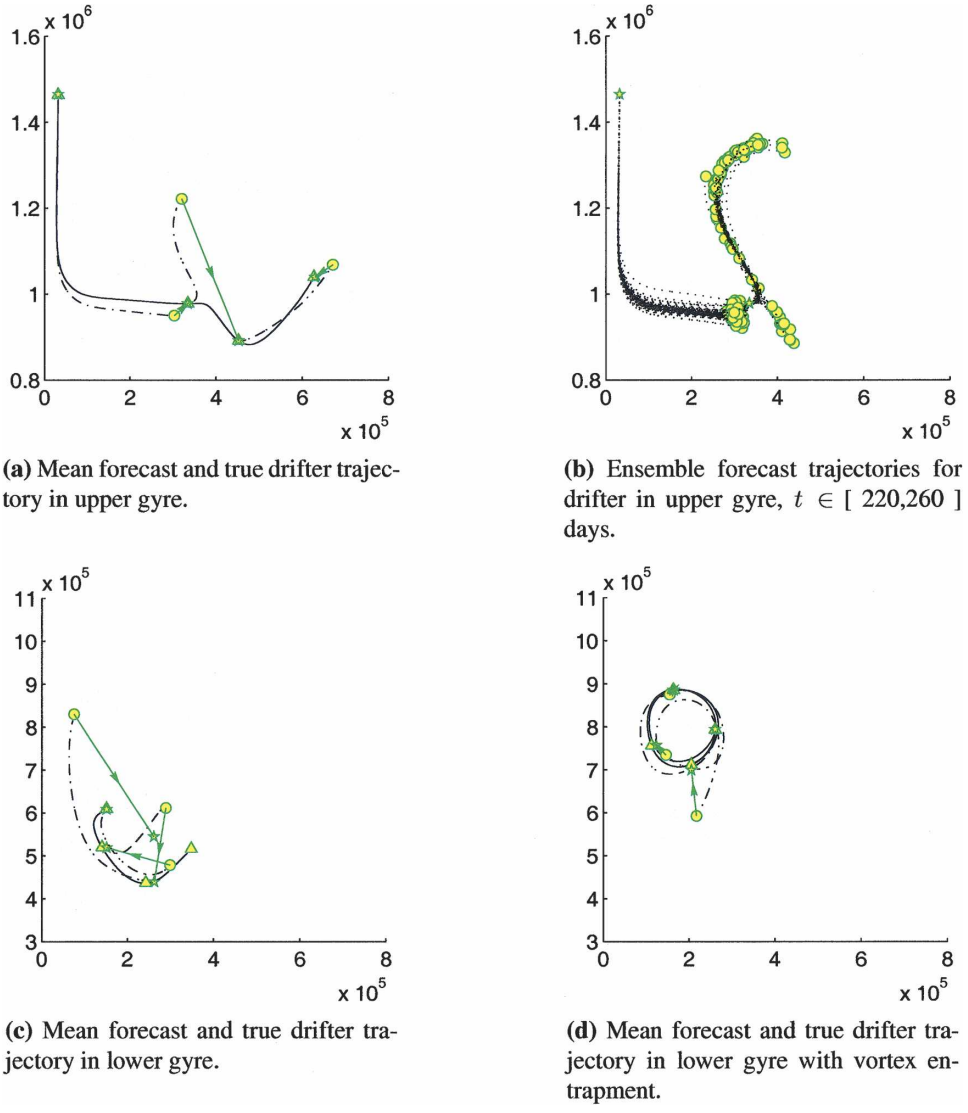

(a) Mean forecast and true drifter trajectory in upper gyre.

(b) Ensemble forecast trajectories for drifter in upper gyre, $t \in [\ 220{,}260\ ]$ days.

(c) Mean forecast and true drifter trajectory in lower gyre.

(d) Mean forecast and true drifter trajectory in lower gyre with vortex entrapment.

FIG. 10. Trajectories of the true and model systems shown for [220, 280] days. Symbols: triangles, $\mathbf{x}_D^t(t_k)$; circles, $\mathbf{x}_D^f(t_k)$ (model state before update); stars, $\mathbf{x}_D^a(t_k)$ (analysis state). Arrows: correction vectors. Solid line: true trajectory; dashed line: model mean trajectory; dotted line: trajectories of individual members.

Both the forecast and true trajectories are shown together with the assimilation steps to highlight the nature of the updates that result in the divergence of the method. The first drifter we consider is presented in Fig. 10a and is located in the upper gyre in the vicinity of the jet. As the drifter emerges from the southerly moving currents in the western boundary, it changes toward an easterly direction advected by the midlatitude jet. An update step is performed at 240 days, reducing the error between the forecast and the true system. Immediately after this update step, the forecast diverges rapidly from the true trajectory. The divergence between the two trajectories is so rapid and in an opposite direction that it hints at the presence of a Lagrangian saddle point in the flow (see Jones and Winkler 2002; Poje et al. 2002). The manifolds (or strictly speaking finite-time attracting and repelling material lines) associated with this saddle point separate the trajectories in phase space such that drifters that are initially located close together but on opposite sides of the manifolds undergo exponentially rapid separation in a finite time. Subsequently, at the next update, a large correction will be necessary to bring the forecast drifter back to its true location, which is observed in our results. Under such a scenario, the evolution of the error covariance matrix as represented by our ensemble

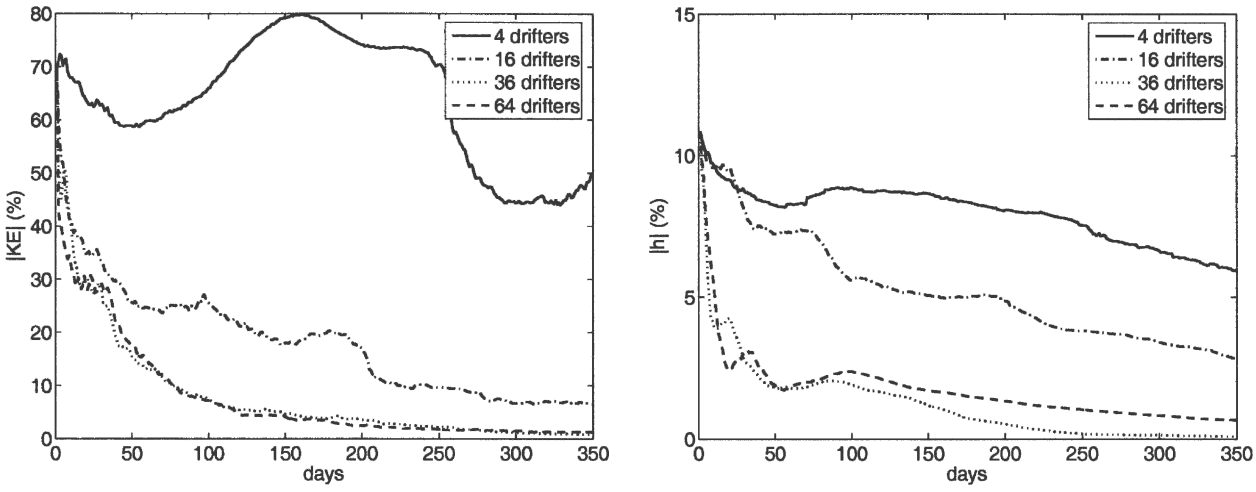

(a) Error in kinetic energy. (b) Error in height field.

FIG. 11. Influence of number of drifters on error convergence for expt 7.

will be highly nonlinear and non-Gaussian. This is reflected in a branching-off of the individual members of our ensemble along the two unstable directions of the saddle point. Such a behavior is illustrated in Fig. 10b where we have plotted the trajectories of our members over the time interval [220, 260] days. The figure clearly illustrates how the trajectories spread out in two opposite directions upon their encounter with the saddle. However, given that the bulk of the realizations spread along the upper branch, the corresponding mean of the ensemble deviates from the truth as we observed in Fig. 10a. The rapid spread in our ensemble causes a modal error distribution, such as the Gaussian distributions we assume, to evolve into a, possibly, bimodal distribution. The more complex form of the error distribution requires a larger ensemble size to provide accurate statistics. More importantly, the variance alone cannot describe the error distribution that results beyond the saddle point, and computing an analyzed state by simply reducing the variance does not necessarily reduce the error. This consequently can lead to divergence of the method, as turns out to be the case in our system. The problems attributed to the exponential drifter separation near the saddle point were also observed in the study of Kuznetsov et al. (2003) using an EKF with a point vortex model. While the EKF clearly breaks down due to the nonlinearities that are not represented in the propagation of errors that are approximated by the TLM [see Ide and Ghil (1998), Miller et al. (1994), Evensen (1997), and Verlaan and Heemink (2001) for analogous results observed within the Eulerian framework], no such linearization is adopted in evolving the errors in the EnKF. The problem in our case, therefore, stems from the use of a finite ensemble size that leads to inaccurate statistics. A common downfall of both the EKF and EnKF, however, is the oversimplification made in using only the variance to compute an optimum state of our system. This assumption will clearly break down in a number of systems with strong nonlinearities.

The other two ill-behaved trajectories are both located in the lower gyre. The trajectory shown in Fig. 10c reveals a chaotic behavior where the filter fails to correct the flow leading to a continuous divergence of the forecast and true drifter trajectories. It is important to emphasize that beyond a time of 260 days, any erroneous updates introduced into the flow by the first drifter can manifest themselves in the divergence of other drifter trajectories and vice versa. The failure of the method locally can therefore lead to spontaneous filter divergence in several other drifters at subsequent times. To support these arguments we consider our final drifter presented in Fig. 10d, which illustrates an entrapment by a coherent vortex. Both the true and forecast trajectories show a recirculating path over [220, 280] days. However, toward the end of the interval, the forecast trajectory diverges, producing a larger update at the final assimilation step. The sudden divergence of the trajectory in this case is believed to have been triggered by the divergence of our first drifter discussed above.

To put the above results into perspective, we note that on a Lagrangian time scale of $T_L = 10$ day intervals, our method for assimilating Lagrangian data is able to drive down the error in our model. The method is degraded for assimilation time intervals greater than

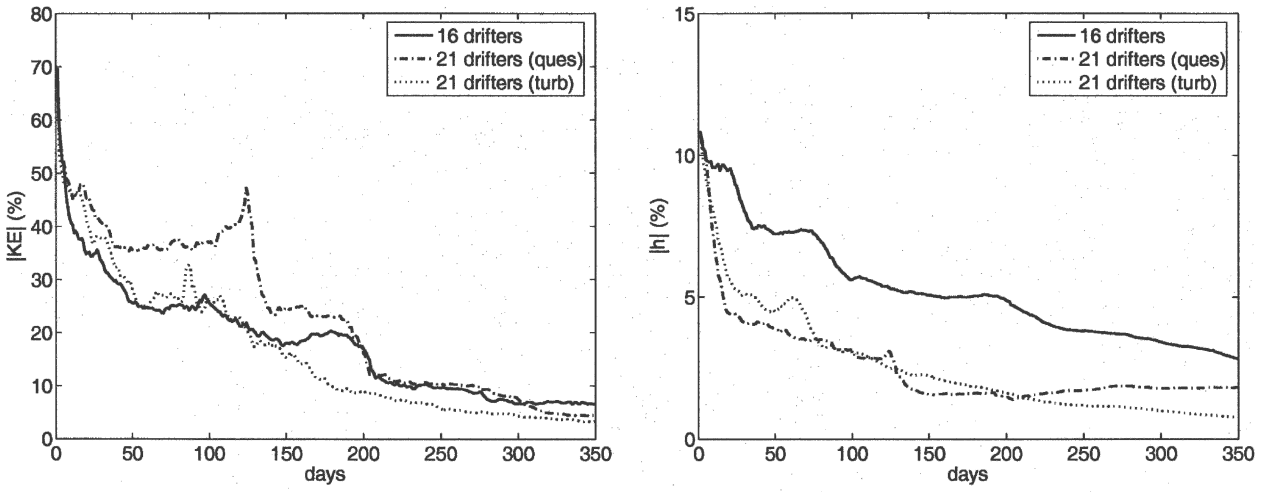

(a) Error in kinetic energy. (b) Error in height field.

FIG. 12. Influence of drifter release location on error convergence for expt 8.

T_L with failure occurring at $2T_L$. Using the same definition of T_L that we have used and similar flow conditions, the method of Özgökmen et al. (2003) required sampling times of $0.2T_L$–$0.5T_L$. The fact that we have not made any approximating assumptions by adopting an augmented system for our formulation has led to a more robust method. As the flow model is refined, however, to resolve more dynamical structures, a corresponding decrease in T_L will occur. Issues associated with the divergence of the scheme caused by an increased encounter of drifters with saddle points could then become important. It is, therefore, useful to develop strategies to circumvent some of the problems raised here. In retrospect, we can point out that the challenges that arise from the saddle points are not specific to our formulation but are an intrinsic feature of Lagrangian data.

e. *Effect of number of drifters and release location*

Another physically important parameter to consider in our Lagrangian data assimilation method is the impact that the number of drifters and their release locations has on the convergence of the scheme. To address these issues, we analyze results from our final two experiments, 7 and 8, from Table 2. In experiment 7, we have used 4, 16, 36, and 64 drifters uniformly distributed in (2×2), (4×4), (6×6), and (8×8) arrays in our simulations, respectively. In all four simulations, the assimilation time interval was fixed at 1 day and an optimum localization radius of $r_{\text{loc}} = 600$ km was chosen for our ensemble containing 80 members. Results for the variation of the errors in terms of the kinetic energy of the flow are presented in Fig. 11a. The sensitive dependence of the rate of convergence of the error on the number of drifters used is immediately apparent. For the case with four drifters, the amount of data assimilated into the model is clearly insufficient to correct the flow. A substantial improvement in the rate of convergence is observed upon increasing our number of drifters to 16. However, the optimum value is achieved with 36 drifters since this produces the maximum reduction in the error with the fewest number of drifters. Similar results are observed for the height field in Fig. 11b. The optimum value of 36 drifters identified here justifies the use of this number in the majority of our experiments discussed so far.

The optimum value identified above corresponds to a uniformly distributed set of drifters. In general, however, it would be more effective to collect more data in dynamically active regions of the flow. To illustrate that the performance of our method does indeed depend on how well we sample the structure within a given flow, we simulate two more cases. In the first case, we introduce additional drifters to the 16 uniformly distributed drifters considered above. The five additional drifters are all released in region "A," the eddy-dominated region of the flow. For the second case, all five drifters are released in region "B," the quiescent part of the flow in the lower gyre. Results presented in Fig. 12a indicate that by adding drifters to region A, the reduction in the error is improved in terms of both the kinetic energy and the height field with a more pronounced correction in the latter. By adding drifters in region B, however, an initial degradation occurs in correcting the kinetic energy of the flow, although the final error at 350 days is comparable to the case in which drifters are released in

region A. In comparison, the opposite scenario is observed, with the height field in which drifters released in region B lead to the highest rate of convergence initially but deteriorate at later times. Our observations, therefore, do indeed confirm that by sampling more of the eddy-dominated regions surrounding the jet, the greatest reduction in both the kinetic energy and height fields can be realized.

5. Conclusions

We have presented a new formulation for assimilating Lagrangian drifter/float data collected at discrete times from the ocean into a primitive equation ocean model where the prognostic flow variables are represented on an Eulerian grid. The principal idea behind the approach was to augment the state vector of the Eulerian flow with the Lagrangian drifter/float coordinates. This augmented system produces an algorithm that is virtually transparent to the Lagrangian nature of the data but one that retains a physically consistent propagation of the errors between the measurements and the flow. We employ the ensemble Kalman filter to take full advantage of the sparse nature of the Kalman gain matrix. This arises from the special form of the observation operator associated with our formulation. We test the method on the reduced-gravity shallow-water system of equations in a parameter range where the flow is unsteady and chaotic drifter trajectories can arise. Working within the framework of the "twin experiment" configuration, we take the average water depth as an unknown parameter in our system. By observing only drifter positions from the "true" system, we are able to correct the error in the entire flow by assimilating these Lagrangian observations. The method relies on providing accurate error statistics from our finite ensemble. We have found that a small ensemble size can degrade the convergence of the method due to noisy correlations between remote sites within our flow domain. We rectified the problem by extending the ideas of localization developed for Eulerian data assimilation to our Lagrangian method.

To test the robustness of the scheme, we have assessed the sensitivity of the method to a number of key physical parameters. We have established that the method remains stable provided the assimilation time interval is on the order of the Lagrangian autocorrelation time scale (T_L). This is a clear improvement over time intervals of $0.2–0.5T_L$ that are quoted by others. In their work, Lagrangian positions from two consecutive observations are used to approximate the Eulerian flow field. These computed velocities are then assimilated into the model. Our approach avoids any approximations associated with such an approach by directly assimilating the drifter positions, thus leading to an overall more robust method. At larger assimilation time intervals, however, the failure of the method can be attributed to the presence of Lagrangian saddle points in the flow that produce an exponentially rapid separation in the forecast and true trajectories. A similar observation was made in our previous study of a point vortex model with an EKF where the saddle point caused the filter to diverge. Stabilizing the method for assimilation steps greater than T_L will therefore require a technique that directly handles the destabilizing effect of the saddle points.

Acknowledgments. H. Salman, L. Kuznetsov, and C. K. R. T. Jones were supported by the Office of Naval Research Grants N00014-93-1-0691 and N00014-03-1-0174; K. Ide was supported by the Office of Naval Research Grant N00014-04-1-0191. The authors thank Dr. Jie Yu for helpful discussions regarding the work presented here.

REFERENCES

Anderson, J. L., 2001: An ensemble adjustment Kalman filter for data assimilation. *Mon. Wea. Rev.,* **129,** 2884–2903.

Aref, H., and M. S. El Naschie, 1995: *Chaos Applied to Fluid Mixing.* Pergamon, 400 pp.

Bauer, S., M. S. Swenson, A. Griffa, A. J. Mariano, and K. Owens, 1998: Eddy-mean flow decomposition and eddy-diffusivity estimates in the tropical Pacific Ocean. *J. Geophys. Res.,* **103,** 855–871.

Bishop, C. H., B. J. Etherton, and S. J. Majumdar, 2001: Adaptive sampling with the ensemble transform Kalman filter. Part I: Theoretical aspects. *Mon. Wea. Rev.,* **129,** 420–436.

Burgers, G., P. J. van Leeuwen, and G. Evensen, 1998: Analysis scheme in the ensemble Kalman filter. *Mon. Wea. Rev.,* **126,** 1719–1724.

Carter, E. F., 1989: Assimilation of Lagrangian data into numerical models. *Dyn. Atmos. Oceans,* **13,** 335–348.

Castellari, S., A. Griffa, T. M. Özgökmen, and P.-M. Poulain, 2001: Prediction of particle trajectories in the Adriatic Sea using Lagrangian data assimilation. *J. Mar. Syst.,* **29,** 33–50.

Chin, T. M., A. C. Haza, and A. J. Mariano, 2002: A reduced-order information filter for multilayer shallow water models: Profiling and assimilation of sea surface height. *J. Atmos. Oceanic Technol.,* **19,** 517–533.

Cohn, S. E., and D. F. Parrish, 1991: The behavior of forecast error covariances for a Kalman filter in two dimensions. *Mon. Wea. Rev.,* **119,** 1757–1785.

Coulliette, C., and S. Wiggins, 2000: Intergyre transport in a wind-driven, quasi-geostrophic double gyre: An application of lobe dynamics. *Nonlinear Processes Geophys.,* **7,** 59–85.

Cushman-Roisin, B., 1994: *Introduction to Geophysical Fluid Dynamics*. Prentice Hall, 320 pp.

Evensen, G., 1994: Sequential data assimilation with a nonlinear quasi-geostrophic model using Monte Carlo methods to forecast error statistics. *J. Geophys. Res.,* **99** (C5), 10 143–10 162.

——, 1997: Advanced data assimilation for strongly nonlinear dynamics. *Mon. Wea. Rev.,* **125,** 1342–1354.

——, 2003: The ensemble Kalman filter: Theoretical formulation and practical implementation. *Ocean Dyn.,* **53,** 343–367.

——, and P. J. van Leeuwen, 2000: An ensemble Kalman smoother for nonlinear dynamics. *Mon. Wea. Rev.,* **128,** 1852–1867.

Ghil, M., and P. Malanotte-Rizzoli, 1991: Data assimilation in meteorology and oceanography. *Advances in Geophysics,* Vol. 33, Academic Press, 141–226.

Griffa, A., L. I. Piterbarg, and T. M. Özgökmen, 2004: Predictability of Lagrangian trajectories: Effects of smoothing of the underlying Eulerian flow. *J. Mar. Res.,* **62,** 1–35.

Hamill, T. M., J. S. Whitaker, and C. Snyder, 2001: Distance-dependent filtering of background error covariance estimates in an ensemble Kalman filter. *Mon. Wea. Rev.,* **129,** 2776–2790.

Heemink, A., M. Verlaan, and A. Segers, 2001: Variance reduced ensemble Kalman filtering. *Mon. Wea. Rev.,* **129,** 1718–1728.

Holland, W. R., 1978: The role of mesoscale eddies in the general circulation of the ocean—Numerical experiments using a wind-driven quasi-geostrophic model. *J. Phys. Oceanogr.,* **8,** 363–392.

Houtekamer, P. L., and H. L. Mitchell, 1998: Data assimilation using an ensemble Kalman flter technique. *Mon. Wea. Rev.,* **126,** 796–811.

——, and ——, 2001: A sequential ensemble Kalman filter for atmospheric data assimilation. *Mon. Wea. Rev.,* **129,** 123–137.

Ide, K., and M. Ghil, 1998: Extended Kalman filtering for vortex systems. Part I: Methodology and point vortices. *Dyn. Atmos. Oceans,* **27,** 301–332.

——, P. Courtier, M. Ghil, and A. Lorenc, 1997: Unified notation for data assimilation: Operational, sequential and variational. *J. Meteor. Soc. Japan,* **75,** 181–189.

——, L. Kuznetsov, and C. K. R. T. Jones, 2002: Lagrangian data assimilation for point vortex systems. *J. Turbul.,* **3,** 053, doi:10.1088/1468-5248/3/1/053.

Jones, C. K. R. T., and S. Winkler, 2002: Invariant manifolds and Lagrangian dynamics in the ocean and atmosphere. *Handbook of Dynamical Systems,* Vol. 2, B. Fiedler, Ed., North-Holland, 55–92.

Kamachi, M., and J. J. O'Brien, 1995: Continuous assimilation of drifting buoy trajectory into an equatorial Pacific Ocean model. *J. Mar. Syst.,* **6,** 159–178.

Kuznetsov, L., M. Toner, A. D. Kirwan, C. K. R. T. Jones, L. H. Kantha, and J. Choi, 2002: The Loop Current and adjacent rings delineated by Lagrangian analysis of near-surface flow. *J. Mar. Res.,* **60,** 405–429.

——, K. Ide, and C. K. R. T. Jones, 2003: A method for assimilation of Lagrangian data. *Mon. Wea. Rev.,* **131,** 2247–2260.

Lavender, K. L., R. E. Davis, and W. B. Owens, 2000: Direct velocity measurements in the Labrador and Irminger Seas describe pathways of Labrador Sea Water. *Nature,* **407,** 66–69.

Mariano, A. J., A. Griffa, T. M. Özgökmen, and E. Zambianchi, 2000: Lagrangian analysis and predictability of coastal and ocean dynamics. *J. Atmos. Oceanic Technol.,* **19,** 1114–1126.

Miller, R. N., M. Ghil, and F. Gauthiez, 1994: Advanced data assimilation in strongly nonlinear dynamical systems. *J. Atmos. Sci.,* **51,** 1037–1056.

Mitchell, H. L., P. L. Houtekamer, and G. Pellerin, 2002: Ensemble size, balance, and model-error representation in an ensemble Kalman filter. *Mon. Wea. Rev.,* **130,** 2791–2808.

Molcard, A., L. I. Piterbarg, A. Griffa, T. M. Özgökmen, and A. J. Mariano, 2003: Assimilation of drifter observations for the reconstruction of the Eulerian circulation field. *J. Geophys. Res.,* **108,** 3056, doi:10.1029/2001JC001240.

Özgökmen, T. M., A. Griffa, and A. J. Mariano, 2000: On the predictability of Lagrangian trajectories in the ocean. *J. Atmos. Oceanic Technol.,* **17,** 366–383.

——, A. Molcard, T. M. Chin, L. I. Piterbarg, and A. Griffa, 2003: Assimilation of drifter observations in primitive equation models of midlatitude ocean circulation. *J. Geophys. Res.,* **108,** 3238, doi:10.1029/2002JC001719.

Pedlosky, J., 1987: *Geophysical Fluid Dynamics.* 2d ed. Springer-Verlag, 710 pp.

Piterbarg, L. I., 2001: Short-term prediction of Lagrangian trajectories. *J. Atmos. Oceanic Technol.,* **18,** 1398–1410.

Poje, A. C., and G. Haller, 1999: Geometry of cross-stream mixing in a double-gyre ocean model. *J. Phys. Oceanogr.,* **29,** 1649–1665.

——, M. Toner, A. D. Kirwan, and C. K. R. T. Jones, 2002: Drifter launch strategies based on Lagrangian templates. *J. Phys. Oceanogr.,* **32,** 1855–1869.

Smolarkiewicz, P. K., and L. G. Margolin, 1998: MPDATA: A finite-difference solver for geophysical flows.. *J. Comput. Phys.,* **140,** 459–480.

Verlaan, M., and A. W. Heemink, 2001: Nonlinearity in data assimilation applications: A practical method for analysis. *Mon. Wea. Rev.,* **129,** 1578–1589.

Wiggins, S., 1992: *Chaotic Transport in Dynamical Systems.* Springer-Verlag, 301 pp.